Oxygenated sunflower biodiesel: Spectroscopic and emissions quantification under reacting swirl spray conditions

Cheng Tung Chong [a, *], Meng-Choung Chiong [b], Jo-Han Ng [c, d], Mooktzeng Lim [e], Manh-Vu Tran [f], Agustin Valera-Medina [g], William Woei Fong Chong [b, d]

[a] China-UK Low Carbon College, Shanghai Jiao Tong University, Lingang, Shanghai, 201306, China
[b] School of Mechanical Engineering, Faculty of Engineering, Universiti Teknologi Malaysia, 81310, Skudai, Johor, Malaysia
[c] Faculty of Engineering and Physical Sciences, University of Southampton Malaysia (UoSM), 79200, Iskandar Puteri, Johor, Malaysia
[d] UTM Centre for Low Carbon Transport in Cooperation with Imperial College London, Universiti Teknologi Malaysia, 81310, Skudai, Johor, Malaysia
[e] Biomass & Plasma Technologies, Renewable Energy & Green Technology, TNB Research Sdn. Bhd., 43000 Kajang, Selangor, Malaysia
[f] School of Engieering, Monash University Malaysia, Jalan Lagoon Selatan, 47500, Bandar Sunway, Selangor, Malaysia
[g] College of Physical Sciences and Engineering, Cardiff University, Wales, UK

ARTICLE INFO

ABSTRACT

The spray combustion characteristics of sunflower (Helianthus annuus) biodiesel/methyl esters (SFME) and 50% SFME/diesel blend and diesel were investigated via a liquid swirl flame burner. The swirl flame was established at atmospheric condition by using a combined twin-fluid atomiser-swirler configuration at varied atomising air-to-liquid ratios (ALR) of 2.0—2.5. Diesel flame showed a sooty flame brush downstream of the main reaction zone, as opposed to the biodiesel flame which showed a non-sooty, bluish flame core. Biodiesel flame exhibited a more intense flame spectra with higher OH* radicals as compared to diesel. Higher preheating main swirl air temperature led to higher NO emission, while CO correspondingly decreased. Sunflower-derived biodiesel generally exhibited slightly higher NO and CO levels than diesel when compared at the same power output, mostly due to higher flame temperature and fuel chemistry effect. By increasing ALR, a significant reduction of NO and CO for both fuel types were concurrently achieved, presenting a strategy to control emissions and atomise biodiesel with higher viscosity under swirl combustion mode.

© 2019 Elsevier Ltd. All rights reserved.

1. Introduction

Clean renewable alternative fuels are currently in high demand to address the energy trifecta to reduce fossil fuel reliance, cut down pollutant emissions and enhance energy supply security. Within the context of liquid alternative fuels, renewable biodiesel shows great promise with recent studies ascertaining its ability to reduce emissions, such as soot, particulate matters and carbon monoxide to varying degrees [1]. This fuel has also been widely applied in the transportation industry around the world by blending it with diesel to diversify fuel sources. Currently, mandates for biodiesel blending exist around Asia for countries such as Malaysia, Indonesia and Thailand with emphasis on B7, B20 and B7 blends, respectively [2]. In the Americas, Argentina, Brazil, Canada

and Colombia each has current biodiesel mandates of B10, B8, B2 and B10, respectively [2]. Meanwhile in the European Union, there are legislations governing the blending for Latvia (B7) Finland (B5.75), Italy (B5), Norway (B3.5) and the Netherlands (B4) [3,4]. Biodiesel production worldwide is estimated to have reached 29.37 billion litres in 2014 [5], and is still showing positive growth trends. The widespread use of biodiesel around the world is partly due to its versatility based on the variety of feedstock used for its production such as soy, rapeseed, canola, coconut, jatropha, palm, waste vegetable oil, animal fats and even algae [6—8].

Stationary combustion devices such as gas turbine, boilers and furnaces are envisaged to be fuel-flexible and operable with alternative fuel under a continuous, swirling spray combustion mode. The performance of alternative liquid fuels, which include biomass-derived biodiesel, bio-oil or blends has been tested by researchers, either using lab-scale swirl flame burner or micro gas turbine. Recently, Chiong et al. [9] examined the effects of unsaturation degree level in biodiesel on emissions under reacting spray

conditions. It was demonstrated that highly unsaturated soybean biodiesel produced noticeably higher nitric oxide (NO) than palm and coconut biodiesels. Kurji et al. [10] investigated the spray combustion characteristics of biodiesel and blends of alternative fuels, notably biodiesel saturated with pyrolysis oil and organic compounds. Higher nitrogen oxide (NO_x) emissions were observed for biodiesels saturated with pyrolysis oil as compared to baseline kerosene at a wide range of equivalence ratio tested, while pure biodiesel produced comparable NO_x emissions as that of kerosene. The differences were based on the solid organic compounds that catalyses carbyne (CH) radical production downstream of the flame zone, leading to an increase in prompt NO_x formation. Panchasara et al. [11] found that biodiesel produced more NO_x than diesel at constant output heat rate. They demonstrated that NO_x for diesel was slightly lower than that of soybean and chicken fat biodiesel, respectively.

The performance of pure biodiesel in swirl flame burner has been investigated by several groups. Chong and Hochgreb [12,13] reported that NO_x emissions were reduced for rapeseed-based biodiesels using a swirl flame burner. The reduction of NO_x was attributed to the oxygen-bound molecule that assists in the local combustion and suppression of prompt NO_x formation, in addition to the atomising air stream injected into the spray core that assists in lowering the flame temperature. The lower peak flame temperature reduces thermal NO formation. Nitric oxide was reduced by approximately 25% when compared with fossil-based fuels. Similar reduction of NO_x was also reported by Hashimoto et al. [14] in a gas turbine burner test that utilises palm biodiesel as fuel injected through a pressure swirl nozzle. Sequera et al. [15] found that soy biodiesel reduced the emissions of NO_x and carbon monoxide (CO) by around 60% and 50%, respectively, against diesel at constant fuel mass flow rate in an atmospheric burner simulating the features of a gas turbine. These works highlight the profound effects of atomisation process on the performance and emissions characteristics of biodiesels.

At system level, biomass-derived fuels have been tested in gas turbine systems. Bolszo and McDonell [16] reported that larger biodiesel droplet sizes led to longer evaporation time and subsequently higher NO_x emissions. Variation of the atomising air-to-liquid ratio (ALR) affects the droplet size, with higher ALR resulting in finer droplets and hence can effectively reduce NO_x. Rehman et al. [17] tested on esterified jatropha oil-diesel blend using a Rover gas turbine IS/60 test rig, and postulated that the higher oxygen content in the fuel elevates the flame temperature and increases NO_x through thermal mechanisms. On the contrary, Krishna [18] reported a reduction of NO_x emission by around 60% when operating a 30 kW Capstone C30 micro gas turbine engine. The findings by Nascimento et al. [19] concurred with [18], where larger biodiesel droplets reduced the temperature reaction in the primary combustion zone, thereby reducing the formation of thermal NO_x and subsequently the overall NO_x levels. However, CO emissions were found to increase for biodiesel, as the higher viscosity resulted in larger fuel droplets and lower volatility of the fuel, leading to greater incidences of incomplete combustion.

The blends of biodiesel with Jet-A1 has been tested in a CFM56-7B turbo-fan engine at the blend ratios of 20% and 40% [20]. A reduction of NO_x and CO emissions for the biodiesel blends was reported, indicating the potential of biodiesel as aviation fuel. In a 30 kW gas turbine engine test, conducted by Habib et al. [21], it was reported that the turbine inlet and exhaust gas temperatures when fuelled with biodiesel and diesel were comparable, but NO emission for biodiesel was substantially lower than that of diesel, indicating that NO_x formation was not dominated by the thermal mechanism. The lower CO emission was attributed to the role of fuel-bound oxygen molecules in biodiesel which oxidises CO into

CO_2, thus reducing the exhaust CO emissions [17,21].

The inconsistencies in biodiesel emissions shown in lab and system level testing are not surprising considering the differences in burner geometry, mode of combustion, pressures, atomisation method and biodiesel composition. Most of the research focus on the main biodiesel feedstock such as palm, soybean and rapeseed under conventional spray conditions. There is a clear literature gap in the testing of other feedstock and modern spray systems. For example, data related to the combustion characteristics of sunflower-based biodiesel is scarce, despite the fact that sunflower (*Helianthus annuus*) oil is the fourth most consumed vegetable oil globally, with an estimation of 0.16 million tonnes of sunflower oil used for biodiesel production in the EU in 2018 [22]. This singles out sunflower oil as a potential major biodiesel feedstock. Although some groups have tested sunflower biodiesel in internal combustion engines [23,24], there is no prior study of sunflower biodiesel combustion under gas turbine operating conditions to-date. In line with the development of fuel-flexible gas turbine technology, rigorous tests are needed to ensure the fuel-system compatibility and operational safety aspects when applying sunflower biodiesel.

In the present work, the combustion and emission characteristics of sunflower-derived methyl esters and its blend with diesel are tested in a model gas turbine swirl burner and compared to baseline diesel. The aims of this study are to investigate the effects of preheated main air temperatures and atomising air-to-liquid ratio (ALR) variation on the combustion and emissions performance at a range of equivalence ratios. It is noted that the former parameter has not been systematically investigated by any model gas turbine burner fuelled with biodiesel, to the best of author's knowledge. Flame imaging and spectroscopic methods are employed to investigate the flame structure and emission spectrum, while a gas analyser is used to measure the post-combustion emissions. The impact of fuel injection control by varying the atomising air and fuel ratio on the post-exhaust emissions is investigated. The experimental data obtained from this study contributes to the database of alternative fuel combustion for gas turbine and serves as validation targets for fuel and flame modelling.

2. Experimental setup

2.1. Swirl burner system

A gas turbine type swirl burner was used to establish spray flames. The liquid fuel was supplied to the nozzle by a peristaltic pump (Longer BQ50-1J) in a silicone tube of 4 mm inner diameter, passing through a chamber that serves as flow damper. The fuel was delivered to an airblast type atomiser (Delavan: SN type-30610-1) for atomisation. The orifice diameters for atomising air and fuel are 1.73 and 0.50 mm, respectively. An axial swirler was placed concentrically at the burner outlet to generate swirl flow. The swirler consists of six straight vanes with the angle of 45° that forms a geometric swirl number of 0.84 based on Eq. (1) [25].

$$S_N = \frac{2}{3}\left[\frac{1-(D_h/D_s)^3}{1-(D_h/D_s)^2}\right]\tan\theta \tag{1}$$

where D_h and D_s are the swirler hub diameter and the swirler diameter, respectively, and θ is the angle of the swirl blade from the centreline. The main air passes through the swirler to form a swirling air flow that envelopes the atomised spray, forming a combustible mixture. The swirler also generates a recirculating flow with high intensity to assist in fuel-air mixing and flame stabilisation.

The main bulk air was preheated using three 500 W rope

heaters (Omega: FGR-100–240 V). The burner wall was insulated with ceramic wool to reduce heat loss. A 1.5 mm K-type thermocouple was placed 10 mm upstream of the burner outlet to acquire the preheated main air flow temperature. This thermocouple signal provides feedback to the PID controller to regulate the heating. The atomising and main air supplies were controlled by air mass flow controllers (Sierra SmartTrak 50). The schematic of the test rig and flow delivery system is shown in Fig. 1.

2.2. Fuel preparation

The fuels used in this study were diesel (Euro 5 standard), sunflower biodiesel/methyl esters (SFME) and 50/50 blend of diesel/SFME. The diesel was purchased from a local petrol station. It is noted that the Malaysian diesel is a pre-blended diesel with 7% palm biodiesel, as stipulated by the national biodiesel blending mandate. Biodiesel can be produced either using catalytic or non-catalytic transesterification methods [26–28]. The usage of alkaline catalyst is known to produce high yield biodiesel in a relatively short period of time [1] and hence is adopted in the present work. The SFME was produced from sunflower cooking oil via the transesterification process. The sunflower oil was first heated up to 60 °C before mixing with methanol and potassium hydroxide (KOH). The mass ratio of sunflower oil:methanol:KOH was fixed at 114:50:1. The mixture was blended for 2 h by using a magnetic stirrer at the temperature of 60 °C and left overnight to allow the produced biodiesel and glycerol to separate. Decanting was carried out to remove glycerol. The decanted biodiesel was heated up to 120 °C for 4 h to allow water and methanol to vaporise. A gas chromatography (Agilent 7820 A) was used to characterise the yield of biodiesel based on EN 14103 standard. The composition of fatty acids for sunflower is shown in Table 1. The main fatty acid compositions of SFME are linoleic and oleic fatty acids, which are unsaturated due to the presence of double bonds.
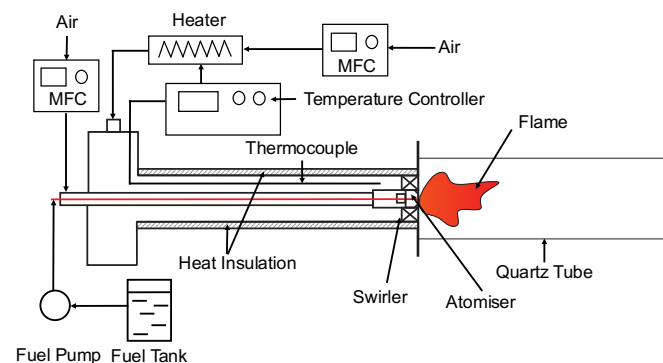

Fig. 1. Schematic diagram of reacting spray rig and flow delivery system.

Table 1
Fatty acid composition of SFME.

Fatty acids	(no. of carbon: double bond)	Composition (%)
Lauric	(C12:0)	0.1
Myristic	(C14:0)	0.1
Palmitic	(C16:0)	6.4
Palmitoleic	(C16:1)	0.1
Heptadecanoic	(C17:0)	0.1
Heptadecenoic	(C17:1)	0.1
Stearic	(C18:0)	3.6
Oleic	(C18:1)	21.7
Linoleic	(C18:2)	66.3
Linolenic	(C18:3)	1.5

2.3. Fuel properties

SFME is more viscous, less volatile and has a higher flash point compared to commercial diesel. Diesel consists of aliphatic and aromatics, while SFME is inherently oxygenated with lower heating value by 12.3% than the former on a mass basis. The approximated molecular weight for SFME and diesel are 294.5 and 226 g/mol, respectively. SFME has higher density than diesel. Blending of the biodiesel and diesel was performed volumetrically at the ratio of 50:50. Kay's mixing rule was utilised for estimating the physical properties of diesel-SFME blends. The physical properties of the blend, including molecular weight, lower heating value and density are estimated by,

$$\Psi = \Sigma \Psi_i x_i \tag{2}$$

where Ψ is the property of the blend, Ψ_i is the respective property of the ith component and x_i is the mass fraction of the ith component [13]. The properties for the fuels are shown in Table 2.

2.4. Measurement techniques

A digital camera (Canon EOS 600D) was utilised to capture the global flame images established at different equivalence ratios through an optically accessible quartz wall. The focal length and exposure time of the camera were set to 4 mm and 1/15 s, respectively. A spectrometer (Avaspec-UL2048 Starline) was utilised to obtain the flame spectrum that spans from ultraviolet to near-infrared range (200–900 nm). The spectrometer was equipped with a 2048 pixel charged-coupled device (CCD) detectors, with a grating resolution of 1200 lines/mm, a slit width of 10 μm, an instrumental wavelength resolution of 0.1 nm, and a signal-to-noise ratio of >10. The signals from the flames were focused onto the CCD detectors of the spectrometer. The time-averaged spectra were obtained with an integration time of 1 s. The focal length was 1 m from the flame.

The post-combustion emissions of NO, CO, CO_2 and O_2 were measured using a gas analyser (KANE Quintox 9106) at the combustor outlet. The sampling was carried out by placing the probe 13 mm inward from the combustor exit. The gas analyser was calibrated using calibration gases prior to measurements. The inlet diameter of the sampling tube is 5 mm and the sampling gas volume is 2 L/min. The NO, CO emissions were measured by chemical sensors in the gas analyser, while the CO_2 emission was calculated based on the measured O_2. The emissions were measured at 5 spatial locations that were equally spaced radially at the burner outlet. The probe samples for 1.5 min at each spatial location to ensure the readings are in steady state condition. The global emission for each test case was obtained by averaging the spatial readings using the area-weighted averaging method. The measurement range, uncertainty and propagated errors of the gas analyser and spectrometer are shown in Table 3.

Table 2
Physical properties for diesel and sunflower biodiesel [6,25].

Properties	Diesel	SFME
C (wt %)	85.0	77.4
H (wt %)	15.0	11.7
O (wt %)	0	10.9
Lower heating value (MJ/kg)	42.6	37.3
Density (kg/m³)	843.3	872.7
Cetane number	50	51
Flash Point (°C)	76	175
Kinematic viscosity (40 °C) (mm²/s)	2.4	4.4
Molecular weight (g/mol)	226.0	294.5

Table 3
Specification of the gas analyser and spectrometer.

Sensor/Instrument	Range	Resolution	Uncertainty	Propagated Error
NO	0–5000 ppm	1 ppm	<100 ppm; ± 5 ppm >100 ppm; ± 5%	±7.5%
CO	0–4000 ppm	1 ppm	<100 ppm; ± 5 ppm >100 ppm; ± 5%	±16.0%
O_2	0–30%	0.01%	±0.2%	±1.3%
CO_2	0–20%	0.1%	±5.0% of reading	±4.2%
Spectrometer	200–1000 nm	0.1 nm	±0.1 nm	±1.3%

2.5. Operating conditions

Three types of fuels were tested in this study, diesel, SFME, and 50/50 diesel-SFME blends. Diesel was chosen as the baseline fuel in this study. The liquid fuel and atomising air were delivered to the burner outlet independently. The main swirling air flow was preheated to 250 °C, prior to mixing with the liquid fuel spray. The fuel flow rate was regulated to achieve the flame power output of 9.3 kW for all test cases. Three atomisation air-to-liquid ratios (ALR) ranging between 2.0 and 2.5 were tested in this study at different equivalence ratios focusing on the fuel-lean region. The range of ALR chosen ensured the sprays were fully developed with a dense cloud of fine droplets. The operating conditions for the flames established at $\phi = 0.65$ and fixed power output of 9.3 kW are shown in Table 4. The effects of preheating main swirl air on post-combustion emissions were conducted at 30, 150 and 250 °C.

3. Result and discussion

3.1. Global flame imaging

The swirl flame images for diesel, SFME and 50/50 diesel-SFME blend established at ALR = 2.5 and three fuel-lean equivalence ratios of $\phi = 0.90$, 0.75 and 0.65 are shown in Fig. 2. The flames established at these conditions are continuous and stable. The variation of the flame appearances and intensities for the fuel types are due to the compositional difference. Diesel flames show luminous orange-yellow flame brushes at the downstream of main reaction zone, whereas SFME flames show mainly bluish flame cores. The yellowish-orange flame brush is indicative of the presence of soot, as expected for diesel based flames, owing to the presence of aromatics which is a precursor to soot formation [25]. It has been shown previously that the production of soot increases linearly with the aromatic contents in the fuel [29,30]. The biodiesel/diesel blends show slightly less intense yellowish flame brushes due to reduced soot concentration when blended with biodiesel, but overall still resemble the pure diesel swirl flame. The biodiesel flames show a different appearance as compared to the diesel flames, notably there is an absence of sooty orange post-reaction

flame brush. This is characteristic of biodiesel flames due to the oxygen attached to the long-chain methyl esters of biodiesels, which assists in local combustion and suppresses the formation of soot [1]. Further, aromatics are not present in biodiesel, thus further reduces the tendency of soot formation.

The bluish flame near the nozzle is the main reaction flame zone, analogous to premixed flame due to the intense mixing between the atomising air and fuel. The sooty flame intensity for diesel is further reduced at fuel-lean region owing to the increase of main bulk air. The sooty flame brush in diesel results in the longer flame length than SFME. Swirl flame is stabilised partly in due to the central toroidal recirculation zone, where the reverse flow is caused by adverse pressure gradients. The flame brush is the region where the spray and air mixes, forming a shear layer. SFME shows distinct shear layers while diesel flame is obscured by the sooty flames.

3.2. Flame emission spectroscopy

3.2.1. Effect of ALR on flame spectra

The flame spectroscopy of SFME and diesel flames are compared at ALR = 2.5 and 2.0 at fixed $\phi = 0.65$, as shown in Fig. 3. At the visible light spectrum range, diesel exhibits a spectrum with a distinct peak at 588 nm and broadband signal from 580 to 900 nm, which is the yellowish-orange band that is attributed to the sooty flame in the post reaction zone. The biodiesel spectra are significantly different from diesel, with distinct peaks at 310, 388, 432, 470 and 515 nm but with the absence of broadband sooty band (>580 nm). The peaks at 310 and 432 nm represent hydroxyl (OH) and CH radicals, respectively [31,32]. The cyanido (CN) radical is shown at 388 nm [33,34] while both 470 and 515 nm represent diatomic carbon (C_2) radicals [35]. However, the C_2 peaks are not evident in the diesel spectra as the dominant soot spectra overshadow the intensity emitted by these radicals, as evident by the larger downstream sooty flame as compared to the bluish main reaction zone for diesel, as shown in Fig. 2. The distinct 588 nm peak in diesel flame is indicative of the trace element of sodium, which is a known contaminant present in diesel. SFME spectra exhibited a 764 nm peak (not shown in diesel flame) that is

Table 4
Operating conditions.

Fuel	ALR	Fuel mass flow rate (g/s)	Atomising air mass flow rate (g/s)	Main swirl air mass flow rate (g/s)
Diesel	2.00	0.22	0.43	4.51
	2.25		0.49	4.46
	2.50		0.54	4.40
SFME	2.00	0.25	0.50	4.27
	2.25		0.56	4.22
	2.50		0.63	4.16
50% SFME/diesel blend	2.00	0.23	0.47	4.39
	2.25		0.53	4.34
	2.50		0.59	4.28

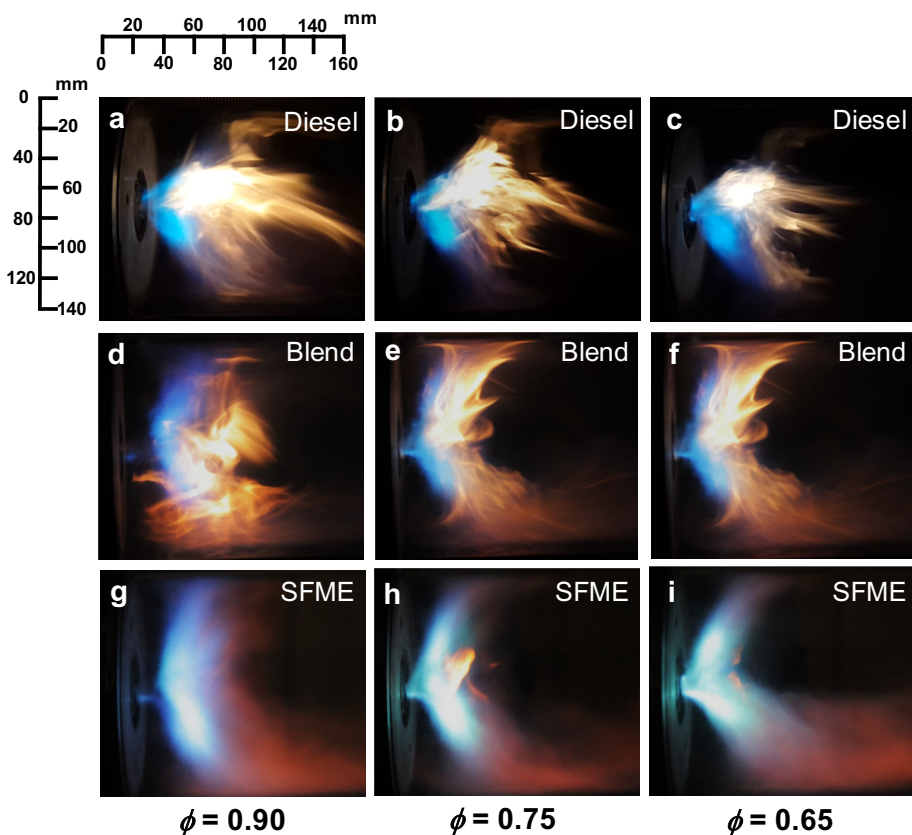* Flames were established at $\phi = 0.65$ and fixed power output of 9.3 kW.

Fig. 2. Flame images for (a–c) diesel, (d–f) 50% diesel/SFME blend and (g–i) SFME swirl flames established at ALR = 2.5 and equivalence ratios of $\phi = 0.65$–0.90.
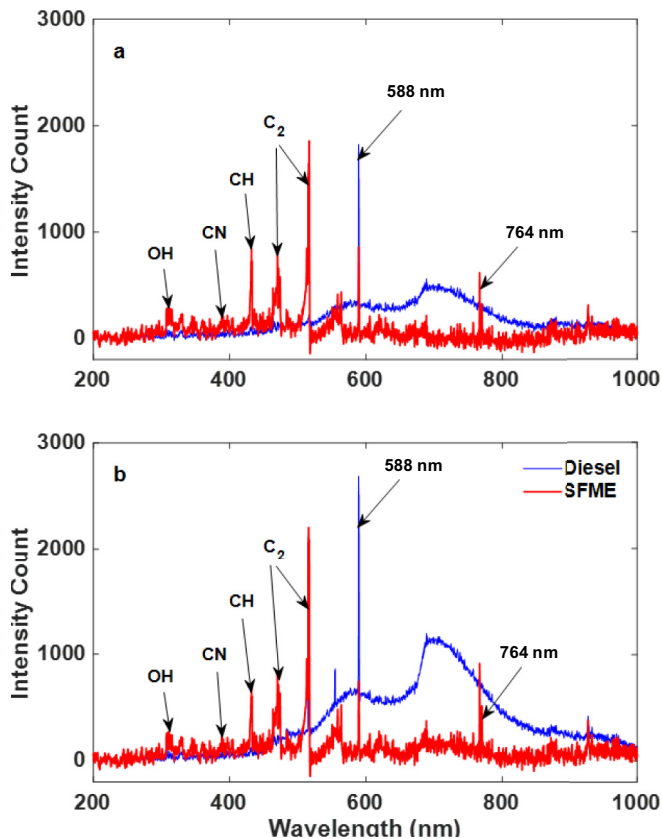

Fig. 3. Flame spectra for diesel and SFME established at ALR = (a) 2.5 and (b) 2.0 at $\phi = 0.65$.

attributable to potassium. Some trace amount of potassium could be left in the biodiesel as the catalyst of potassium hydroxide was used during the transesterification process.

By varying the ALRs, the intensity of the flame changes despite both flames were established at the global equivalence ratio of 0.65. This is reflected in the sooty band of >580 nm for diesel, where ALR = 2.5 shows a significant reduction in spectrum intensity as compared to ALR = 2.0. At higher ALR, the higher throughput of atomising air resulted in greater air momentum, thus increasing the mixing with spray droplets and promoted atomisation and evaporation. Therefore, the sooty yellowish orange band is significantly reduced for diesel flame for ALR = 2.5. For SFME, the spectra at both ALRs are similar with the notable absence of radiation from the sooty flames.

3.2.2. Radical emission intensities

The OH and CH radicals emitted from the flames for diesel and SFME as a function of equivalence ratio at ALR = 2.5 are shown in Fig. 4a and b respectively. It can be observed that these radical intensities are highest at near stoichiometric conditions due to increased flame temperatures and higher flame intensities [32,36]. At the fuel-lean region where more air was being introduced, the flame temperature and burning intensity were lower, causing the signal intensity count to reduce correspondingly. In the flame, hydrocarbon fuel undergoes reaction of hydrogen abstraction followed by the β-scission to create a pool of H radical that is essential for the production of OH radical, as shown in reactions R1-R4 [37–39].
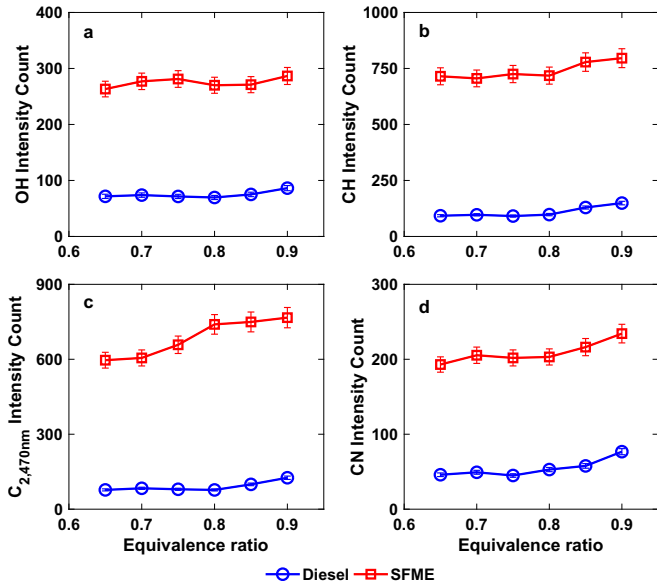
$$O + H + M \rightarrow OH + M \tag{R1}$$

$$O + H2 \rightarrow H + OH \tag{R2}$$

Fig. 4. Intensity counts of (a) OH (b) CH (c) $C_{2,470nm}$ (d) CN radicals for diesel and SFME at a range of equivalence ratio and fixed ALR = 2.5.

$$H + O_2 \rightarrow O + OH \tag{R3}$$

$$H + HO_2 \rightarrow OH + OH \tag{R4}$$

The CH radical can be produced from CH_2 or ethynyl (C_2H) radical as shown in reactions R5-R8 [40–42]. The CH_2 radicals can be produced from the *bis*-allylic sites in biodiesel, thus biodiesel generally produces more CH_2 radicals than diesel [9,43]. This explains the higher CH intensity for biodiesel compared to diesel as shown in Fig. 4b.

$$CH_2 + H \rightarrow CH + H_2 \tag{R5}$$

$$CH_2 + OH \rightarrow CH + H_2O \tag{R6}$$

$$CH_2 + O \rightarrow CH + OH \tag{R7}$$

$$C_2H + O \rightarrow CO + CH \tag{R8}$$

The OH and CH radicals for SFME are approximately 73% and 87% higher than diesel respectively when compared at the same equivalence ratio. The increase in OH and CH radicals in SFME swirl flame can partly be attributed to the increase of fuel mass flow rate [32,36]. The fuel mass flow rate for SFME was increased to compensate for its lower caloric value against diesel, and to enable comparison of flames at the same power output. With more biodiesel fuel being introduced, more hydrogen atoms and CH_2 radicals are available for the elementary reactions R1-R8 to produce more OH and CH radicals. Hence, the flame spectra for SFME shows higher OH and CH radicals intensities compared to that of diesel. Further, the flame temperature is another factor that affects the production of OH and CH radicals [32,36]. Higher flame temperatures increase chemical reaction rates [42]. Biodiesel was shown to have higher adiabatic temperature against that of diesel owing to higher O/C atomic ratio [44], which assists in the formation rate of OH and CH radicals [32,36].

C_2 is another prominent radical in SFME swirl flame as shown in the flame spectra (Fig. 3) and intensity plot (Fig. 4c). The formation of C_2 radical is highly dependent on CH, CH_2 and C radicals, based on reactions R9-R11 [45]. In addition to the higher CH radical in

SFME spray flame, the long SFME carbon chain is another factor that promotes the formation of C_2 radical, since more carbon atoms are introduced to the elementary reactions R9 and R10.

$$CH_2 + C \rightarrow C_2 + H_2 \tag{R9}$$

$$CH + C \rightarrow C_2 + H \tag{R10}$$

$$CH + CH \rightarrow C_2 + H_2 \tag{R11}$$

The CN radical is primarily formed from HCN by reacting with oxygen atoms and OH radicals, as shown by reactions R12-R13 [33]. The primary path for HCN formation is given by R14-R15, which involves the reaction between CH radical and nitrogen in the air and NO [39,46]. Similar to the C_2 radical, the formation of HCN and CN radicals are highly dependent on the availability of CH and CH_2 radicals [39,46]. The relatively abundant CH_2 radical in SFME directly contributes to higher CN intensity as compared to those of diesel, as shown in Fig. 4d.

$$HCN + O \rightarrow CN + OH \tag{R12}$$

$$HCN + OH \rightarrow CN + H_2O \tag{R13}$$

$$CH + N_2 \rightarrow HCN + N \tag{R14}$$

$$CH + NO \rightarrow HCN + O \tag{R15}$$

3.3. Post-combustion emissions

3.3.1. Effect of preheating main air

The effect of preheating main air on the emissions of NO for diesel and SFME is shown in Fig. 5. In general, the increase of main air temperature resulted in an increase of NO for both fuel types, with SFME showing marginally higher NO than diesel. The NO emissions for SFME increases by approximately 18.3% and 59.5% on average for elevated temperatures of 150 °C and 250 °C. Thermal NO is largely responsible for the formation of NO due to the high flame temperature. For preheated air at 250 °C, the NO emission for biodiesel at the range of equivalence ratio of 0.75−0.9 is higher, as a
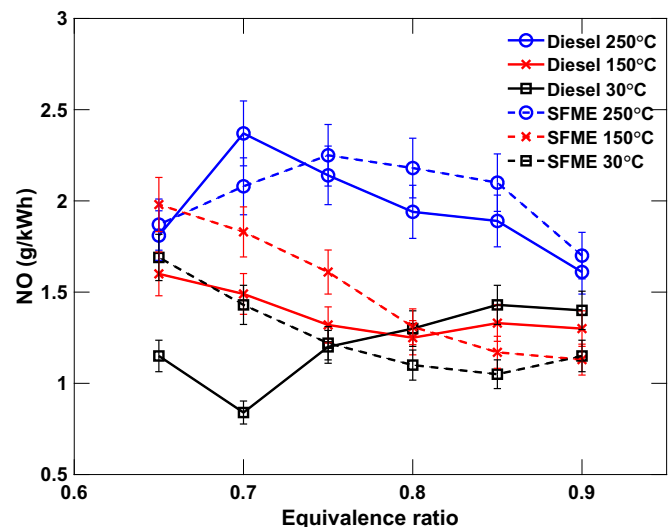

Fig. 5. Emissions of NO against equivalence ratio for diesel and SFME at ALR = 2.5 for preheated air temperatures of 30, 150 and 250 °C.

result of higher flame temperatures as the mixture approaches stoichiometric conditions. Oxygenated biodiesels are also known to produce higher flame temperatures [44]. The preheated air provided the energy to cause the molecules to vibrate more rigorously and assist in chemical reactions.

At lower preheating main air temperature of 30 °C and 150 °C, the biodiesel cases show higher NO emissions at fuel-lean conditions, in particular for equivalence ratios below 0.75. At a lower flame temperature, prompt NO formation is more dominant. The CH radicals, which have been shown to be more abundant in biodiesels (Fig. 4b), initiate the prompt NO formation through reaction $CH + N_2 \rightarrow HCN + N$. The HCN radical is then oxidised into NO via the reaction $HCN \rightarrow CN \rightarrow NCO \rightarrow NO$ [47]. Another NO contributor is the CN radical which is shown to be higher in biodiesel (Fig. 4d). Hence, it can be observed that the main air temperature and the chemistry of the fuels are dominant factors that affect NO emissions.

The CO emissions show a reverse trend to NO, where CO level decreases with increasing main air temperature, as shown in Fig. 6. The CO emissions are reduced by a factor of three when the main air is preheated from 30 to 250 °C, indicating the effect of preheating main air temperature is evident in reducing CO due to the energy provided by the heated air that promotes complete combustion. Both flames show increasing CO emissions with the increase of equivalence ratio, as the addition of fuel into the mixture resulted in the lack of oxygen and residence time for more complete combustion. At fuel-lean conditions, higher swirl flow intensity due to higher air flow rate resulted in increased mixing intensity, leading to lower CO. SFME emitted higher CO than diesel across the range of equivalence ratios tested for temperatures of 150 and 250 °C, most probable cause is the lower fuel volatility and higher viscosity of biodiesel that resulted in inferior spray quality and larger fuel droplets. The pockets of incomplete fuel/air mixture resulted in incomplete combustion, in particular for mixtures approaching stoichiometric conditions. Meanwhile, the higher CH and C_2 radicals in biodiesel may be another contributing factor to higher CO

due to reactions with OH and NO, as shown in reactions R16-R18 [48].

$$C_2 + OH \rightarrow CO + CH \tag{R16}$$

$$CH + O_2 \rightarrow CO + OH \tag{R17}$$

$$C_2 + NO \rightarrow CO + CN \tag{R18}$$

The effect of preheating main air on CO_2 emissions is shown in Fig. 7. The CO_2 emitted from both fuels under swirling conditions increases with increasing temperature and equivalence ratio. The higher CO_2 emissions at elevated temperature is due to the
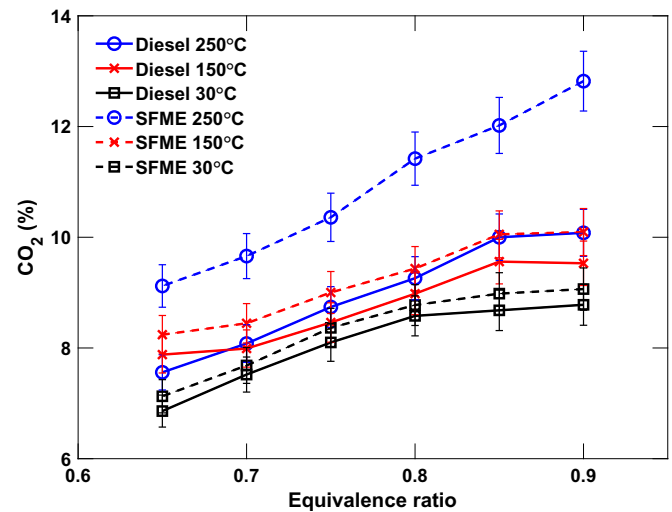

Fig. 7. Emissions of CO_2 against equivalence ratio for diesel and SFME at ALR = 2.5 for preheated air temperatures of 30, 150 and 250 °C.
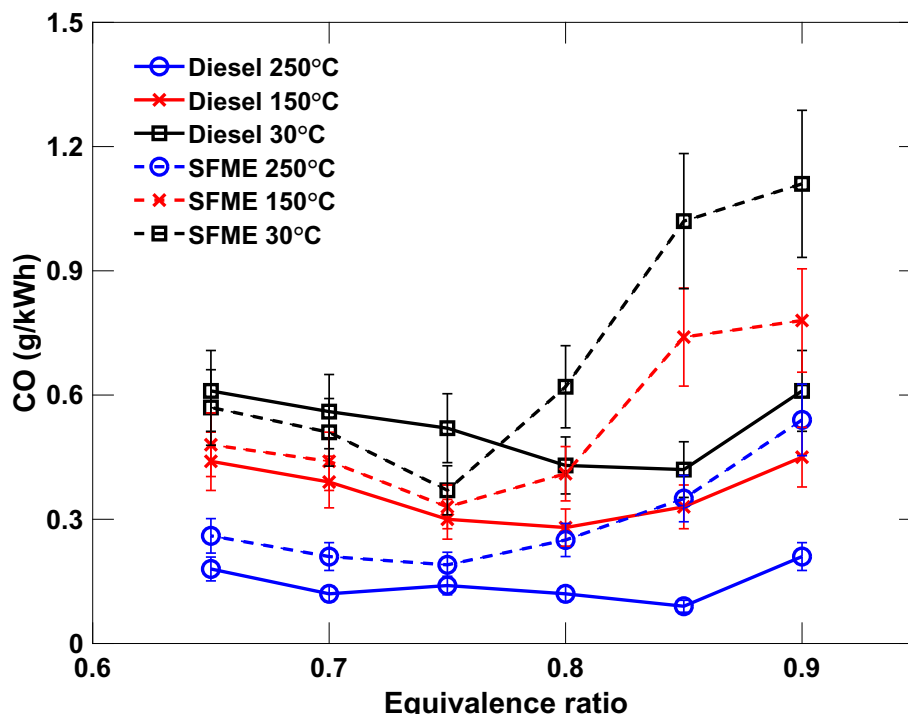

Fig. 6. Emissions of CO against equivalence ratio for diesel and SFME at ALR = 2.5 for preheated air temperatures of 30, 150 and 250 °C.

promotion of CO_2 conversion from CO as a result of higher oxidation rate [47], thus showing the reverse trend for CO. SFME is consistently emitting higher CO_2 compared to baseline diesel, owing to the conversion of oxygen in biodiesel molecule into CO_2 during combustion and partly due to the slightly higher fuel mass flow rate.

3.3.2. Effect of atomising air-to-liquid ratio (ALR)

The effect of atomising air-to-liquid ratio on the emissions for SFME, diesel and 50% SFME is shown in Fig. 8. The increase of ALR from 2 to 2.5 resulted in a concurrent decrease of NO and CO emissions, indicating the dominating effect of ALR on emissions. This concurs with previous study [16] where the increase of ALR resulted in lower NO in a micro gas turbine combustor that operates with a twin-fluid atomiser. It is noted that despite ALR = 2 is sufficient in generating a fully developed spray, the emission levels for NO and CO are the highest, for both diesel and biodiesel among the ALR tested. The NO emissions for biodiesel is higher than diesel for ALR = 2−2.25, but both flames converged to lowest emission levels at ALR = 2.5. Whereas for CO emissions, biodiesel is consistently higher than diesel for the range tested. The blend's emissions

for NO and CO largely fell in between biodiesel and diesel. The higher NO emissions for biodiesel shown at lower ALR is due to a higher flame temperature. The relatively lower atomising air momentum resulted in slightly larger droplets at the spray periphery, as was quantified previously by utilising the same twin-fluid type atomiser [49]. Some of these larger droplets may not have fully vaporised and were convected downstream of the atomiser, forming local hot spots due to secondary diffusion flame, thus increasing the local temperature [47]. Likewise, the higher CO emissions at lower ALR were due to incomplete vaporisation of droplets, resulting in incomplete combustion.

At higher ALR, more atomising air was supplied to the atomiser outlet. The high momentum of atomising air contained high kinetic energy that assists in breaking up the spray, resulting in the increase of distance between droplets and increasing the interaction between the air and the droplets [50]. Finer droplets were generated at high ALR, thus increased the rate of vaporisation and subsequently aided in the mixing between vapour and air in the spray core. Apart from promoting mixing, the high amount of air lowered the spray core temperature, thus reducing the formation of thermal NO. Lower CO emissions at high ALR was due to improved mixing
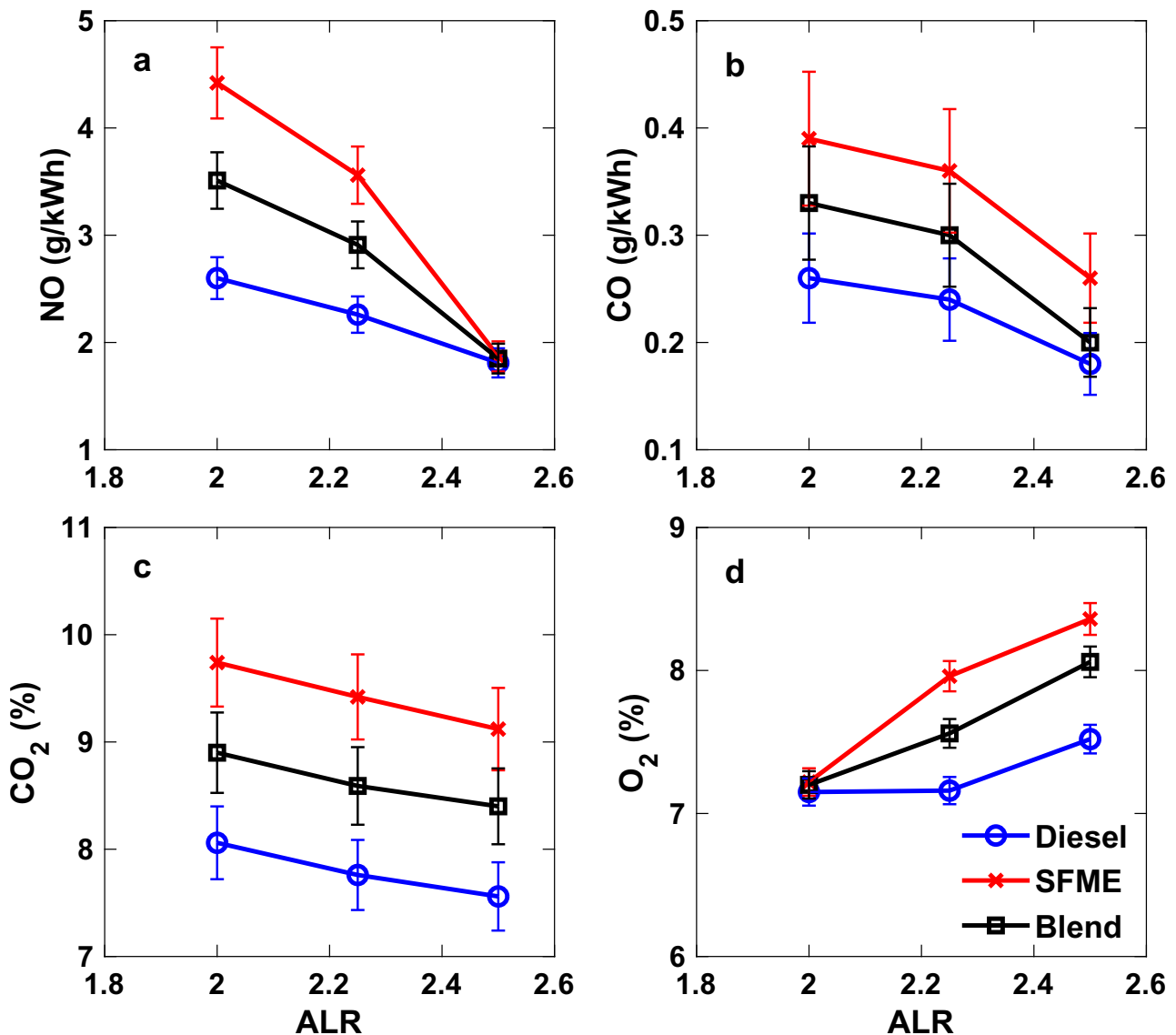

Fig. 8. Emissions of (a) NO (b) CO (c) CO_2 and (d) O_2 as a function of ALR for diesel, SFME and 50/50 diesel/SFME blend at $\phi = 0.65$ and main air temperature of 250 °C.

and more complete combustion, which is analogous to a premixed flame. Fig. 8c shows the CO_2 emissions from the combustion of biodiesel is higher than those of diesel. Lower ALR resulted in higher CO_2 emissions. This could be due to higher combustion temperature at lower ALR accelerates the oxidation rate of CO into CO_2 [47]. For O_2, the reduction of ALR resulted in lower O_2, as more oxygen was consumed for oxidising CO into CO_2. Meanwhile, the combustion of biodiesel produced higher O_2 level than those of blend and diesel fuels due to the higher inherent oxygen content in the fuel.

4. Conclusion

The spray combustion characteristics of sunflower biodiesel (SFME) and 50% diesel/SFME blend were compared against diesel under the same power output of 9.3 kW. Diesel flame showed a distinct luminous orange-yellow flame at the downstream of the main reaction zone due to the presence of soot, while SFME showed an intense bluish flame core without the sooty flame brush. From the spectroscopic measurement, biodiesel flame spectra exhibited distinct peaks consisting of OH, CN, CH and C_2 radicals at 310, 388, 432, 470 and 515 nm, respectively. The intensities of these radicals were higher than those in diesel. Diesel spectra showed the sooty broadband at >580 nm which was absent in biodiesel flame.

The NO emission level was higher while the CO was correspondingly lower for both flames at elevated temperature of 250 °C. Biodiesel exhibited higher NO level than diesel due to higher flame temperatures. Further, a higher level of CH, CN and C_2 radicals in biodiesel also promoted the formation of NO. The higher CO emissions for biodiesel can be attributed to lower fuel volatility and incomplete combustion of pockets of fuels owing to larger droplet or inadequate mixing. By increasing the ALR, the NO and CO levels can be effectively reduced with finer spray and improved mixing. This work shows that in spite of the slightly higher emissions of NO and CO for sunflower biodiesel, the variation of the injector's atomising air-fuel ratio can serve as an active control measure to reduce pollutant emissions.

Acknowledgement

References

[1] Chiong MC, Chong CT, Ng J-H, Lam SS, Tran M-V, Chong WWF, et al. Liquid biofuels production and emissions performance in gas turbines: a review. Energy Convers Manag 2018;173:640—58.

[2] Naylor RL, Higgins MM. The rise in global biodiesel production: implications for food security. Glob Food Sec 2017;16:75—84.

[3] Barisa A, Romagnoli F, Blumberga A, Blumberga D. Future biodiesel policy designs and consumption patterns in Latvia: a system dynamics model. J Clean Prod 2015;88:71—82.

[4] Arshad M, Abbas M. Water sustainability issues in biofuel production. In: Arshad M, editor. Perspect. Water usage biofuels prod. Springer; 2018.

[5] Abomohra AE-F, Jin W, Tu R, Han S-F, Eid M, Eladel H. Microalgal biomass production as a sustainable feedstock for biodiesel: current status and perspectives. Renew Sustain Energy Rev 2016;64:596—606.

[6] Hoekman SK, Broch A, Robbins C, Ceniceros E, Natarajan M. Review of biodiesel composition, properties, and specifications. Renew Sustain Energy Rev 2012;16:143—69.

[7] Kadir WNA, Lam MK, Uemura Y, Lim JW, Lee KT. Harvesting and pre-treatment of microalgae cultivated in wastewater for biodiesel production: a review. Energy Convers Manag 2018;171:1416—29.

[8] Sales EA, Ghirardi ML, Jorquera O. Subcritical ethylic biodiesel production from wet animal fat and vegetable oils: a net energy ratio analysis. Energy Convers Manag 2017;141:216—23.

[9] Chiong MC, Chong CT, Ng J-H, Tran M-V, Lam SS, Valera-Medina A, et al. Combustion and emission performances of coconut, palm and soybean methyl esters under reacting spray flame conditions. J Energy Inst in press, doi.org/10.1016/j.joei.2018.07.003.

[10] Kurji H, Valera-Medina A, Runyon J, Giles A, Pugh D, Marsh R, et al. Combustion characteristics of biodiesel saturated with pyrolysis oil for power generation in gas turbines. Renew Energy 2016;99:443—51.

[11] Panchasara HV, Simmons BM, Agrawal AK, Spear SK, Daly DT. Combustion performance of biodiesel and diesel-vegetable oil blends in a simulated gas turbine burner. J Eng Gas Turbines Power 2009;131:031503.

[12] Chong CT, Hochgreb S. Spray flame structure of rapeseed biodiesel and Jet-A1 fuel. Fuel 2014;115:551—8.

[13] Chong CT, Hochgreb S. Flame structure, spectroscopy and emissions quantification of rapeseed biodiesel under model gas turbine conditions. Appl Energy 2017;185:1383—92.

[14] Hashimoto N, Ozawa Y, Mori N, Yuri I, Hisamatsu T. Fundamental combustion characteristics of palm methyl ester (PME) as alternative fuel for gas turbines. Fuel 2008;87:3373—8.

[15] Sequera D, Agrawal AK, Spear SK, Daly DT. Combustion performance of liquid biofuels in a swirl-stabilized burner. J Eng Gas Turbines Power 2008;130:032810.

[16] Bolszo CD, McDonell VG. Emissions optimization of a biodiesel fired gas turbine. Proc Combust Inst 2009;32:2949—56.

[17] Rehman A, Phalke DR, Pandey R. Alternative fuel for gas turbine: esterified jatropha oil-diesel blend. Renew Energy 2011;36:2635—40.

[18] Krishna CR. Performance of the Capstone C30 microturbine on biodiesel blends. 2007.

[19] Nascimento MAR, Sierra RGA, Silva Lora EE, Rendon MA. Performance and emission experimental evaluation and comparison of a regenerative gas microturbine using biodiesel from various sources as fuel. J Energy Resour Technol 2011;133:022204.

[20] Timko MT, Herndon SC, De La Rosa Blanco E, Wood EC, Yu Z, Miake-Lye RC, et al. Combustion products of petroleum jet fuel, a fischer-tropsch synthetic fuel, and a biomass fatty acid methyl ester fuel for a gas turbine engine. Combust Sci Technol 2011;183:1039—68.

[21] Habib Z, Parthasarathy R, Gollahalli S. Performance and emission characteristics of biofuel in a small-scale gas turbine engine. Appl Energy 2010;87:1701—9.

[22] Flach B, Lieberz S, Lappin J, Bolla S, Phillips S. EU-28. Biofuels Annual 2018. GAIN Report Number: NL8027.

[23] Efe Ş, Ceviz MA, Temur H. Comparative engine characteristics of biodiesels from hazelnut, corn, soybean, canola and sunflower oils on DI diesel engine. Renew Energy 2018;119:142—51.

[24] Dueso C, Muñoz M, Moreno F, Arroyo J, Gil-Lalaguna N, Bautista A, et al. Performance and emissions of a diesel engine using sunflower biodiesel with a renewable antioxidant additive from bio-oil. Fuel 2018;234:276—85.

[25] Chong CT, Hochgreb S. Spray combustion characteristics of palm biodiesel. Combust Sci Technol 2012;184:1093—107.

[26] Demirbas A. Comparison of transesterification methods for production of biodiesel from vegetable oils and fats. Energy Convers Manag 2008;49:125—30.

[27] García-Martínez N, Andreo-Martínez P, Quesada-Medina J, de los Ríos AP, Chica A, Beneito-Ruiz R, et al. Optimization of non-catalytic transesterification of tobacco (Nicotiana tabacum) seed oil using supercritical methanol to biodiesel production. Energy Convers Manag 2017;131:99—108.

[28] Gebremariam SN, Marchetti JM. Biodiesel production through sulfuric acid catalyzed transesterification of acidic oil: techno economic feasibility of different process alternatives. Energy Convers Manag 2018;174:639—48.

[29] Tian B, Chong CT, Fan L, Ng J-H, Zhang C, Hochgreb S. Soot volume fraction measurements over laminar pool flames of biofuels, diesel and blends. Proc Combust Inst 2019;37:877—84.

[30] Cignoli F, De Iuliis S, Zizak G. Soot load versus aromatic concentration in diesel oil premixed flames. Fuel 2001;80:945—55.

[31] Józsa V, Kun-balog A. Spectroscopic analysis of crude rapeseed oil flame. Fuel Process Technol 2015;139:61—6.

[32] Higgins B, Mcquay MQ, Lacas F, Rolon JC, Darabiha N, Candel S. Systematic measurements of OH chemiluminescence for fuel-lean , high-pressure , premixed , laminar flames. Fuel 2001;80:67—74.

[33] Juchmann W, Latzel H, Shin DI, Peiter G, Dreier T, Volpp H-R, et al. Absolute radical concentration measurements and modeling of low-pressure CH4/O2/NO flames. Proc Combust Inst 1998;27:469—76.

[34] Watanabe H, Yamamoto J ichiro, Okazaki K. NOx formation and reduction mechanisms in staged O2/CO2 combustion. Combust Flame 2011;158:1255—63.

[35] Stamatoglou P. Spectral analysis of flame emission for optimization of combustion devices on marine vessels. Lund University; 2014.

[36] Higgins B, Mcquay MQ, Lacas F, Candel S. An experimental study on the effect of pressure and strain rate on CH chemiluminescence of premixed fuel-lean methane/air flames. Fuel 2001;80:1583—91.

[37] Wang C, Wu W. Roles of the state-resolved OH(A) and OH(X) radicals in microwave plasma assisted combustion of premixed methane/air: an exploratory study. Combust Flame 2014;161:2073—84.

[38] He L, Guo Q, Gong Y, Wang F, Yu G. Investigation of OH* chemiluminescence and heat release in laminar methane—oxygen co-flow diffusion flames.

Combust Flame 2019;201:12–22.

[39] Zhao D, Yamashita H, Kitagawa K, Arai N, Furuhata T. Behavior and effect on NOx formation of OH radical in methane-air diffusion flame with steam addition. Combust Flame 2003;44:98–9.

[40] Hossain A, Nakamura Y. A numerical study on the ability to predict the heat release rate using CH*chemiluminescence in non-sooting counterflow diffusion flames. Combust Flame 2014;161:162–72.

[41] Joklik RG, Daily JW, Pitz WJ. Measurements of CH radical concentrations in an acetylene/oxygen flame and comparisons to modeling calculations. Symp Combust 1988;21:895–904.

[42] Elsamra RMI, Vranckx S, Carl SA. CH(A2) formation in hydrocarbon combustion: the temperature dependence of the rate constant of the reaction C2H + O2 -> CH(A2) + CO2. J Phys Chem A 2005;109:10287–93.

[43] Bazooyar B, Hashemabadi SH, Shariati A. NOx formation of biodiesel in utility power plant boilers; Part B. Comparison of NO between biodiesel and petrodiesel. Fuel 2016;182:323–32.

[44] Jha SK, Fernando S, To SDF. Flame temperature analysis of biodiesel blends and components. Fuel 2008;87:1982–8.

[45] Kojima J, Ikeda Y, Nakajima T. Basic aspects of OH(A), CH(A), and C2(d) chemiluminescence in the reaction zone of laminar methane-air premixed flames. Combust Flame 2005;140:34–45.

[46] Sun ZW, Li ZS, Konnov AA, Aldén M. Quantitative HCN measurements in CH4/N2O/O2/N2 flames using mid-infrared polarization spectroscopy. Combust Flame 2011;158:1898–904.

[47] Lefebvre AH, Ballal DR. Gas turbine combustion: alternative fuels and emissions. third ed. CRC Press; 2010.

[48] Matsui Y, Nomaguchi T. Spectroscopic study of prompt nitrogen oxide formation mechanism in hydrocarbon-air flames. Combust Flame 1978;32: 205–14.

[49] Chong CT, Hochgreb S. Effect of atomizing air flow on spray atomization of an internal-mix twin-fluid atomizer. At Sprays 2015;25:657–73.

[50] Chiu H-H, Liu TM. Combustion science and technology group combustion of liquid droplets. Combust Sci Technol 1977;17:127–42.